**Rare Metal Materials and Engineering**

Available online at **www.rmme.ac.cn**

Science Press

**Cite this article as:** Rare Metal Materials and Engineering.

ARTICLE

DOI: 10.12442/j.issn.1002-185X.20240458.

# The influence of Y content on the formability and friction wear of Fe-Cr-C-B-Ti cladding metals

**Jianbo Guo [1], Zhengjun Liu [1], Yunhai Su [1*]**

[1] *School of Materials Science and Engineering, Shenyang University of Technology, Shenyang 110870, China*

**Abstract:** The failure of mechanical parts is mainly caused by three types of reasons: wear, corrosion, and fatigue. Among these three failure modes, wear and tear of mechanical components notably increase energy consumption and lead to substantial economic losses. Preparation of Fe-Cr-C-B-Ti-Y wear resistant cladding metals by plasma cladding method. The wear performance of cladding metals was analyzed using the MLS-23 rubber wheel wet sand wear tester. XRD, SEM, EBSD, and TEM were employed to examine the phase composition and microstructure of the cladding metals, followed by a discussion on the cladding metals strengthening and wear mechanisms. The results indicate that the microstructure of Fe-Cr-C-B-Ti-Y cladding metals is composed of austenite γ-Fe+$M_{23}(C,B)_6$ eutectic carbide+TiC hard phase. As the amount of $Y_2O_3$ added increases, the hardness and wear of the deposited metal show a trend of first increasing and then decreasing. When the $Y_2O_3$ content is 0.4%, the precipitation of TiC hard phase and $M_{23}(C,B)_6$ type eutectic carbides reaches its maximum, and the grain size in the microstructure is the smallest. The forming performance of the cladding metal is the best, and the wetting angle is the smallest, only 52.2 °. At this point, the rockwell hardness value of the cladding metal is 89.7 HRC, and the wear weight loss is 0.27g. The wear mechanism of cladding metals is mainly abrasive wear, and the material removal process involves micro cutting and plowing.

**Key words:** Fe-Cr-C-B; cladding metal; nano-$Y_2O_3$; ceramic phase; Wear resistance

With the continuous development of science and technology, the performance requirements of materials used in tool manufacturing and mechanical engineering are gradually increasing ; mechanical parts, tools and molds in the course of use in addition to a few because of brittle fracture damage, most due to material fatigue or wear and failure. Fe-Cr-C surfacing alloy is a common wear-resistant alloy. The hard phases such as MC, $M_7C_3$ and $M_{23}C_6$ generated in the alloy structure are usually dispersed to improve the abrasion resistance of alloy [1-2].

The wear resistance of Fe-based hardfacing alloys comes from the coordination between the carbide hard phase with high hardness and the matrix with strong toughness. Nagarathnnam, Komvopoulos et al. [3] designed Fe-Cr-W-C powder and successfully prepared iron-based alloy cladding layer. Research has found that the coating is composed of small primary austenite dendrites and a eutectic structure of austenite and M7C3 type, with a Vickers microhardness of up to 8 GPa. Debta et al. [4] deposited TiC-Co-n$Y_2O_3$ cladding layer on Ti-6Al-4V alloy plate by TIG cladding method. With the addition of nano $Y_2O_3$, the melting efficiency of TIG welding is improved, and TiC particles are completely melted, transforming into slender dendrites during the solidification process. After adding nano $Y_2O_3$, the alloy obtained excellent mechanical properties. The average microhardness has slightly increased, while the friction coefficient has significantly decreased. Compared with TiC-Co deposited metal, the wear of TiC-Co-2%$Y_2O_3$ coating is almost four times reduced. The addition of nano $Y_2O_3$ effectively purifies grain boundaries, improves grain structure, and enhances the fracture toughness of the deposited metal. In the sliding wear test, the brittle cracking and extraction of TiC particles were suppressed, and the absolute wear resistance of the coating was improved. Shi et al. [5] found by adding $Y_2O_3$ to Fe-Cr-C-Nb surfacing alloy that $Y_2O_3$ can act as a heterogeneous nucleation core for the

Received date:

Foundation item: NSFC(××××)

Corresponding author: ×××, Ph.D., Professor, Rare Metal Material and Engineering Press, Northwest Institute for Nonferrous Metal Research, Xi'an 710016, P. R. China, Tel: 0086-29-86231117, E-mail: rmme@c-nin.com

MC, refining the hard phase MC and making its distribution more uniform. At the same time, the wear resistance of the deposited alloy has been improved.

Rare earth elements are a series of metal elements with similar physical and chemical properties. It benefits from its unique electronic structure, strong chemical reactivity, and large ion size, which enable it to efficiently play a role in refining grain size during metal cladding [6]. Introducing rare earth elements appropriately into the cladding metals can effectively promote grain refinement, reduce crack tendency, and comprehensively improve the hardness, corrosion resistance, and wear resistance of the surface layer of the cladding metals [7-9]. Adding nano-$Y_2O_3$ to the cladding metals can serve as a heterogeneous nucleation point for the secondary refinement of $M_{23}C_6$ eutectic carbides in the hard phase. This study prepared Fe-Cr-C-B-Ti-Y wear-resistant cladding metals by plasma cladding, and investigated the effect of rare earth oxide $Y_2O_3$ (0 wt.% - 0.5 wt.%) on the microstructure and wear resistance of Fe-Cr-C-B-Ti cladding metals.

## 1 Material and methods

### 1.1 Preparation of cladding metals

Select conventional Q235 carbon structural steel as the matrix material, and its chemical composition is listed in Tab. 1. To prepare for welding, an angle grinder is used for comprehensive rust removal and polishing, ensuring the removal of rust, impurities, and oxide film to clean the surface.

Tab. 1 The chemical composition of Q235(wt%)

| element | C | Si | Mn | P | S |
|---|---|---|---|---|---|
| content | 0.12-0.20 | <0.30 | 0.30~0.70 | <0.045 | <0.045 |

The main components of the composite strengthening alloy include chromium nitride (61.5% Cr, 18% N), chromium powder (99% Cr), boron iron powder (18% B), high silicon iron powder (75% Si), reduced iron powder, titanium powder (99% Ti), etc. The particle size of alloy powder is 80 to 100 mesh. The design composition is Fe-25Cr-5C-2B-6Ti-Y (0 wt.% - 0.5 wt.%) cladding metals alloy. Mix and stir the alloy powder of each element in the strengthened alloy system evenly. Using a ball mill to grind the particles evenly and finely, the metal powder is highly absorbent of moisture, and damp flux cored welding wires are prone to defects such as pores and cracks [10]. Therefore, the powder should be dried in advance. Fig. 1 shows the SEM image of the base powders and the schematic diagram of plasma welding. The prepared alloy powder is deposited onto the surface of Q235 steel plate using a plasma welding machine to prepare the corresponding cladding metals. The cladding process parameters are shown in Tab. 2.

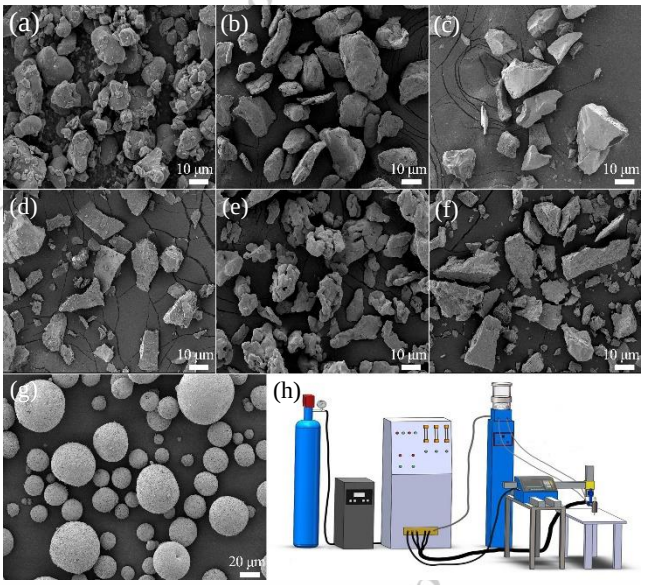


Fig. 1 SEM image of mixed powder and schematic diagram of plasma welding

Tab. 2 Welding process parameters

| Arc voltage (V) | Welding current (A) | Welding speed (m/h) | Gas flow rate (L/min) |
|---|---|---|---|
| 32 | 190 | 10 | 20 |

### 1.2 Organizational and performance testing

After mechanical processing of the melted metal, under the radiation of pure Cu target material, the tube voltage was 40 kV, the tube current was 30 mA, the scanning step was 2 °/min, and the scanning range was 0 °~100 °. The phase structure of the melted metal was characterized using X-ray diffraction (XRD) diffractometer. The microstructure, phase distribution, and worn surface morphology of the cladding metals were carefully observed using the S-3400N scanning electron microscope (SEM), and the specific composition of the precipitated phase was identified using the energy dispersive spectroscopy (EDS) equipped with the SEM. Using electron backscatter diffraction (EBSD) technology to analyze microstructure information such as grain size and volume percentage of precipitates inside the cladding metals. The selected area electron diffraction (SAED) of FEI TalosF200X transmission electron microscope (TEM) was used to determine the type and structure of precipitates in the cladding metals, and the composition of precipitates was determined using an energy dispersive spectrometer. The surface hardness measurement of the cladding metals was carried out using the Rockwell hardness tester (HRS-150, Shanghai, China). The lateral microhardness of the cladding metals was tested using a Vickers hardness tester (TMVP-1T, Beijing, China) under a load of 1 Kg and a loading time of 15 s. The MLS-23 rubber wheel wet sand wear tester was used for abrasive wear experiments. The experimental parameters were: rubber wheel rotation speed 240 rpm, quartz sand particle size 20-50 mesh, wear time 5 min, maximum positive pressure of 23 kg for the rubber wheel.

## 2 Results and Discussion

### 2.1 Phase structure

Fig. 2 shows the XRD patterns of cladding metals with different Y contents added. From the Fig. 2, it's evident that the cladding metals' matrix retains an austenitic structure (γ-Fe), with the primary hard phase consisting of $M_{23}(C,B)_6$ eutectic carbides and TiC. Compared with the cladding metals without $Y_2O_3$ addition, the diffraction peak of TiC is more pronounced, because $Y_2O_3$, as the core of heterogeneous nucleation, can improve the nucleation rate and promote the formation of TiC hard phase. The introduction of Y does not alter the phase composition but predominantly influences by refining the microstructure and purifying grain boundaries.

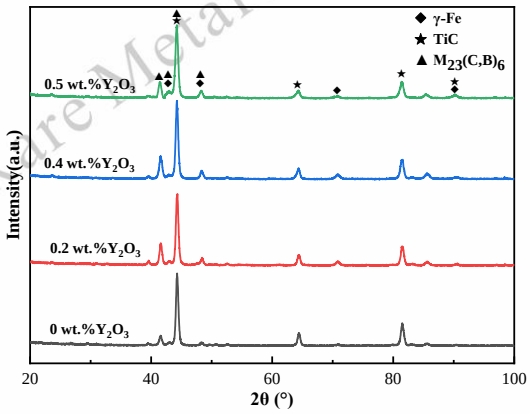


Fig. 2 XRD spectrum of cladding metals with different $Y_2O_3$ content

### 2.2 Microstructure

Good wettability and small contact angle are necessary conditions to ensure interface bonding. According to the Young Dupre equation [11], it can be inferred that:

$$cos\theta=(\sigma_{sg}-\sigma_{sl})/\sigma_{lg}$$

In the formula $\theta$ for wetting angles; $\sigma_{sg}$ is the surface tension at one end of the base material; $\sigma_{sl}$ is the tension at the interface between cladding metals and base metal; $\sigma_{lg}$ is the surface tension of the liquid. When the surface tension of the cladding metals is small, the contact angle is small, and the wettability is good. That is to say, the wetting effect of the metal liquid on the substrate surface can be improved by reducing the surface tension of the metal liquid [12].

Incorporating rare earth elements into cladding metals enhances powder flowability and wettability in metal matrix composites, thereby reducing porosity and other defects, and ultimately fostering improved weld shape formation [13]. Fig. 3 shows the morphology of cladding metals with different $Y_2O_3$ contents. As the amount of $Y_2O_3$ added increases from 0 wt.% to 0.4 wt.%, the splashing rate of the cladding metals gradually decreases, the amount of smoke and dust decreases, the formability of the cladding metals is good, and wetting angle gradually decreases to 52.2 °. When the amount of $Y_2O_3$ added is 0.5 wt.%, cracks and pores begin to appear on the surface of the cladding metals, resulting in poor formability and an increase in wetting angle to 82.0 °. It is obvious that the appropriate addition of $Y_2O_3$ can promote the formation of cladding metals.

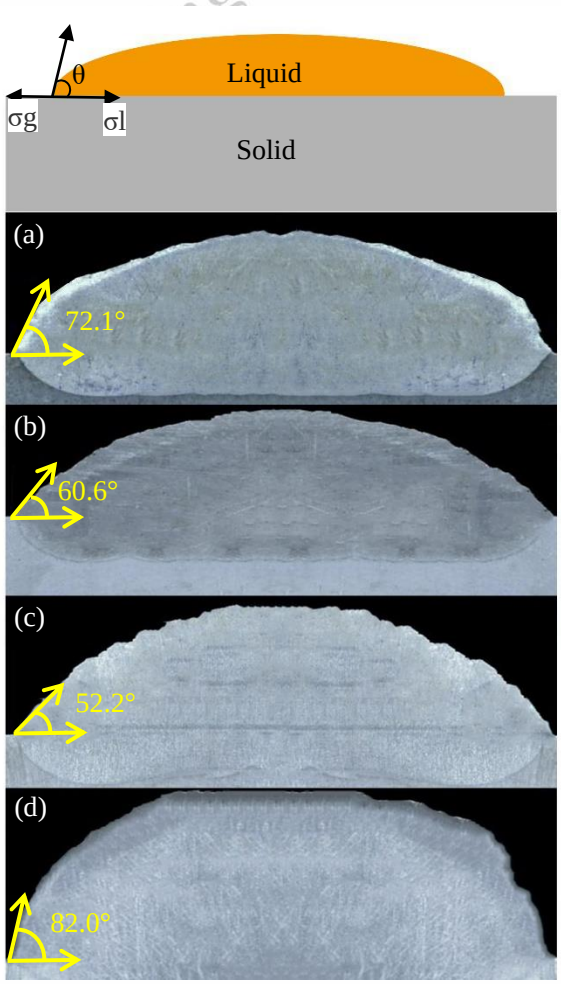


Fig. 3 Morphology of cladding metals forming with different $Y_2O_3$ content: (a) 0 wt.%, (b) 0.2 wt.%, (c) 0.4 wt.%, (d) 0.5 wt.%

Fig. 4 shows the microstructure of cladding metals with different $Y_2O_3$ contents. From the Tab. 3, it can be observed that the cladding metals has a typical eutectic structure, with the matrix composed of austenite γ-Fe, the precipitated phase consists of a network of eutectic carbides $M_{23}(C,B)_6$ and black block like TiC precipitates. When the amount of $Y_2O_3$ added is 0.4 wt.%, the microstructure grains of the cladding metal are the smallest, changing from coarse dendrites to equiaxed grains. Compared with the absence of $Y_2O_3$, it hinders the migration of grain boundaries and refines the microstructure of the cladding metals. The precipitation of $M_{23}(C,B)_6$ eutectic carbides and TiC hard phases reaches its maximum value and is evenly distributed. This phenomenon is attributed to the incomplete melting characteristics of high melting point $Y_2O_3$ during the welding process; The partially melted $Y_2O_3$ particles serve as effective heterogeneous nucleation centers in the deposited metal, enhancing nucleation activity and promoting the effective generation of TiC hard phases. A large amount of dispersed TiC particles can effectively anchor grain boundaries, suppress their movement, and thus achieve grain refinement [14]. When the $Y_2O_3$ content increases to 0.5 wt.%, the structure transforms into coarser dendritic crystals, mainly because excessive $Y_2O_3$ element reduces the fluidity of the melt, weakens convection, and slows down the cooling rate of

the melt, providing time for the full growth of dendrites [15]. This indicates that an appropriate amount of $Y_2O_3$ element addition is crucial for refining grain size and enhancing the wear resistance of the cladding metals.

Tab. 3 Energy spectrum analysis (wt.%)

| $Y_2O_3$ content | | B | C | Ti | Cr | Fe | Y |
|---|---|---|---|---|---|---|---|
| 0 wt.% | A | 5.40 | 3.64 | 0.77 | 14.68 | 75.51 | - |
| | B | 2.87 | 4.08 | 0.60 | 28.27 | 64.18 | - |
| | C | 1.94 | 14.36 | 50.82 | 10.54 | 22.34 | - |
| 0.2 wt.% | A | 5.28 | 3.59 | 0.64 | 13.76 | 76.60 | 0.13 |
| | B | 2.37 | 4.22 | 0.83 | 27.11 | 65.20 | 0.27 |
| | C | 1.27 | 14.26 | 54.63 | 9.89 | 19.71 | 0.24 |
| 0.4 wt.% | A | 5.98 | 3.52 | 0.46 | 10.53 | 79.17 | 0.34 |
| | B | 5.12 | 5.34 | 0.91 | 22.75 | 65.47 | 0.41 |
| | C | 3.35 | 15.43 | 62.89 | 7.83 | 10.11 | 0.39 |
| 0.5 wt.% | A | 5.03 | 3.47 | 0.67 | 11.68 | 78.87 | 0.28 |
| | B | 5.59 | 6.14 | 1.22 | 22.18 | 64.40 | 0.47 |
| | C | 3.06 | 14.76 | 63.29 | 8.51 | 9.77 | 0.61 |

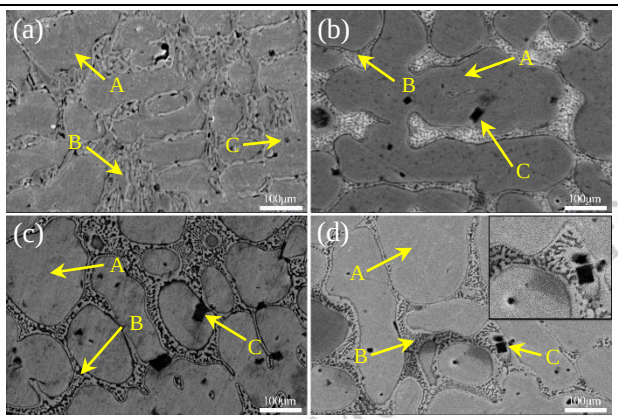


Fig.4 Microstructure of cladding metals forming with different $Y_2O_3$ content: (a) 0 wt.%, (b) 0.2 wt.%, (c) 0.4 wt.%, (d) 0.5 wt.%

Fig. 5 shows the STEM image of the hard phase of a cladding metals with a Y content of 0.4 wt.%. From Fig. 5a, it can be observed that the hard phase exhibits a block like morphology, with black strip-shaped particles distributed in its internal area. In Fig. 5b, region A shows a typical FCC structure, with TiC as hard phase and a crystal band axis of [011]. In Fig. 5c, it is calibrated and determined to be $Y_2O_3$. In Fig. 5d, the two phases overlap, indicating that TiC and $Y_2O_3$ can form heterogeneous nucleation interfaces. In this mechanism, $Y_2O_3$ acts as an effective nucleation center, not only promoting the generation of TiC, but also refining the grain size and facilitating the precipitation of eutectic carbides. In summary, the addition of $Y_2O_3$ significantly enhances the wear resistance of the cladding metals.

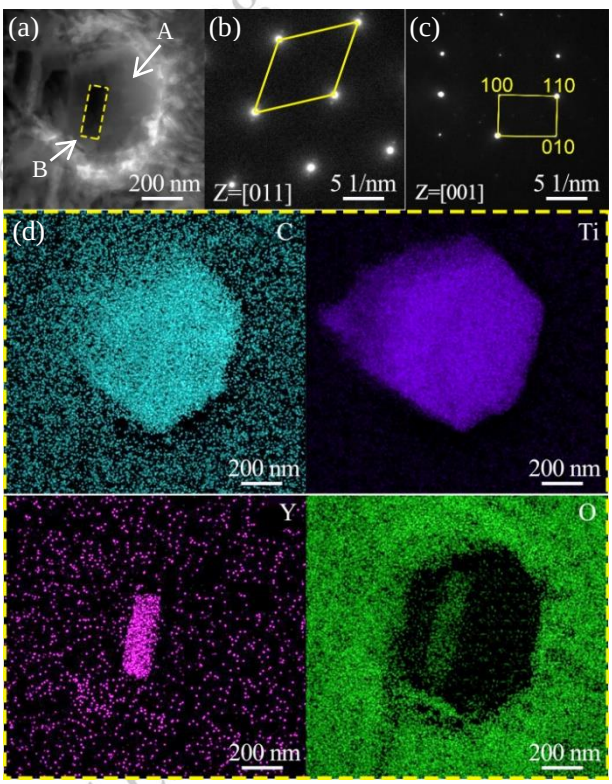


Fig. 5 $Y_2O_3$ content is 0.4wt.% STEM images and SAED images of the cladding metal: (a) TiC BF image, (b) region A SAED image, (c) region B SAED image, (d) EDS element distribution

Fig. 6 shows the EBSD IPF diagrams and grain size statistics of different $Y_2O_3$ content cladding metals. As shown in the fig. 6, when the amount of $Y_2O_3$ added increases to 0.4 wt.%, the grain size of cladding metal is significantly refined. Specifically, the average grain size increases from the initial 3.42 μm significantly reduced to 2.35 μm. Meanwhile, the grain size distribution tends to be more uniform. However, after the content of $Y_2O_3$ was further increased to 0.5 wt.%, the grain size of the cladding metal showed a reverse change, increasing to 3.87 μm. And it shows a non-uniform increase in grain size. The relationship between grain size and yield strength can be described based on the Hall Petch equation [16]:

$$\sigma_s=\sigma_i+kd^{-1/2}$$

In the formula, $\sigma_s$ indicates the yield stress of the material, $\sigma_i$ represents the lattice resistance encountered by dislocation movement, k is a proportional constant, and d represents the grain size. The formula reveals that the smaller the grain size, the higher the yield stress of the material. Generally speaking, the hardness of a material is positively correlated with its strength. Therefore, by appropriately adding $Y_2O_3$ element to refine the grain structure of the cladding metals, it directly promotes a significant increase in hardness. However, when the amount of $Y_2O_3$ added exceeds the appropriate range, the microstructure of the cladding metals will become coarsened, and this structural change will lead to a decrease in hardness performance.

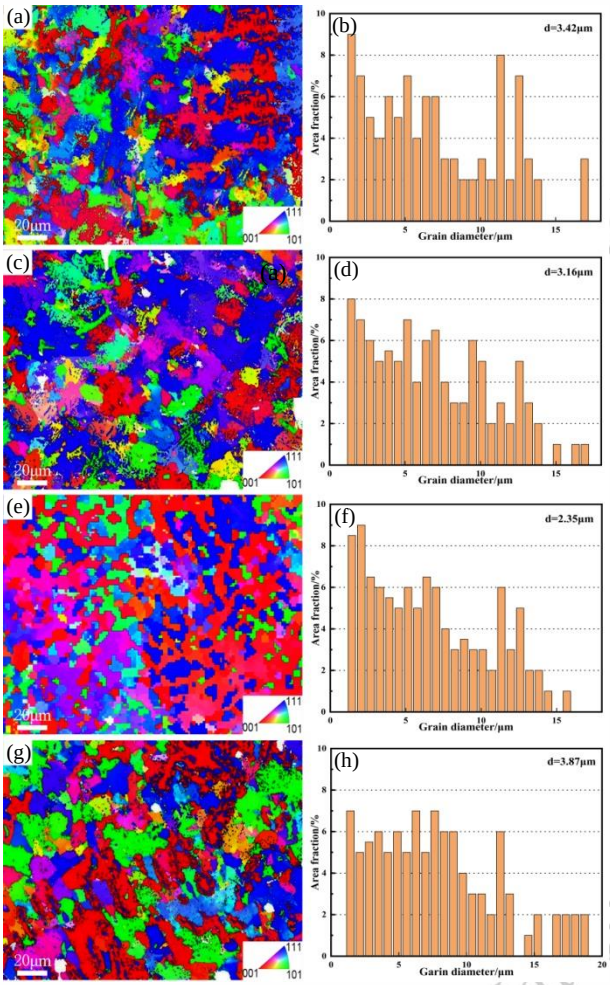


Fig. 6 IPF diagrams and grain size statistics of different $Y_2O_3$ content scladding metals: (a) and (b): 0 wt.%, (c) and (d): 0.2 wt.%, (e) and (f): 0.4 wt.%, (g) and (h): 0.5 wt.%

### 2.3 Analysis of hardness

Fig. 7 shows a histogram of the changes in rockwell hardness of cladding metals with different $Y_2O_3$ contents added. As shown in the fig. 7, it can be observed that the effect of $Y_2O_3$ content on the hardness of the cladding metals shows a trend of first increasing and then decreasing. The hardness of the cladding metals is 61.0 HRC without the addition of $Y_2O_3$. When the amount of $Y_2O_3$ added was adjusted to 0.4 wt.%, the rockwell hardness significantly increased to 89.7 HRC, with a hardness increase of 47%. From the observation of microstructure, it can be concluded that the increase in the content of $Y_2O_3$ does not significantly affect the volume fraction of matrix austenite in the cladding metals. In contrast, the volume fraction of $M_{23}(C,B)_6$ eutectic carbides and TiC precipitates increased significantly. These high-density $M_{23}(C,B)_6$ eutectic carbides and TiC precipitates are uniformly and finely dispersed in the matrix, which is the reason for the enhanced hardness of the cladding metals. However, when the content of $Y_2O_3$ continues to increase to 0.5 wt.%, the flowability of the molten pool of the cladding metals begins to weaken, making it difficult to effectively discharge inclusions and gases, thereby leading to defect formation. At the same time, the cooling rate of the molten pool of the cladding metals slows down, prolonging the time for tissue formation, ultimately resulting in a coarse structure of the cladding metals. The combined effect of these factors has led to a decrease in the hardness of the cladding metals [17].

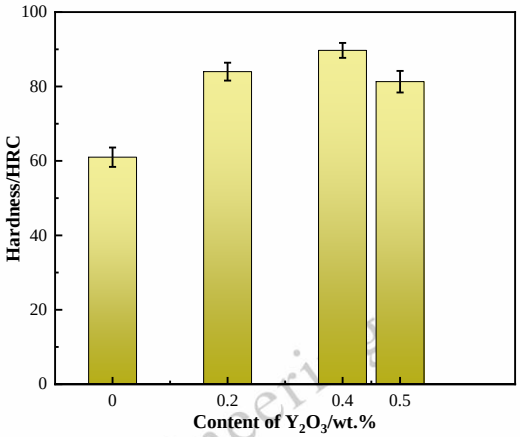


Fig. 7 Surface rockwell hardness of cladding metals with different $Y_2O_3$ content

Fig. 8 shows the variation of microhardness on the side of the cladding metals with different $Y_2O_3$ contents. As shown in the fig. 8, with the increase of the amount of $Y_2O_3$ added, the microhardness of the cladding metals undergoes a process of first increasing and then decreasing. When the content of $Y_2O_3$ reaches 0.4 wt.%, microhardness of the cladding metals reached its peak at 1003 HV, which increased by 35.7% compared to the situation without the addition of $Y_2O_3$. However there, the microhardness of matrix material Q235 is relatively low, about 270 HV. Near the surface area of the cladding metals, the microhardness gradually increases, mainly due to the dilution effect of the substrate, which reduces the precipitation of $M_{23}(C,B)_6$ eutectic carbides in the cladding metals, thereby suppressing the increase in microhardness to a certain extent.

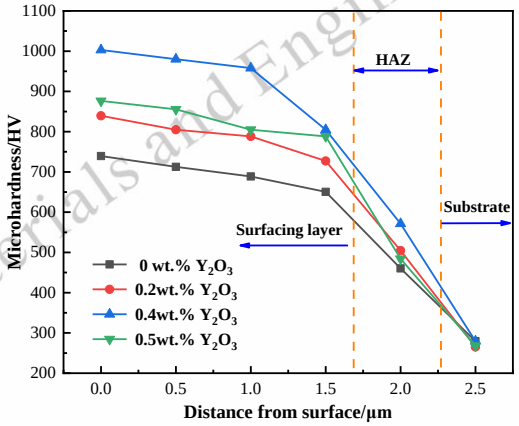


Fig 8 Microhardness of side of cladding metals with different $Y_2O_3$ content

### 2.4 Analysis of wear resistance

Fig. 9 shows the changes in wear weight loss of cladding metals with different $Y_2O_3$ contents. The Fig. 9 shows that the wear weight loss of the cladding metals decreases first and then increases with the increase of $Y_2O_3$ content. When the $Y_2O_3$ content reaches 0.4 wt.%, the wear performance is optimal and the loss of mass is minimal, only 0.27 g. Compared with the non $Y_2O_3$ added cladding metals, the wear resistance is improved by 55.56%. However, as the content $Y_2O_3$ further increases to 0.5 wt.%, the wear weight loss significantly increases and the wear resistance weakens. The wear resistance of the cladding metals varies with the amount of $Y_2O_3$ added, which is consistent with the trend of hardness change. The appropriate addition of $Y_2O_3$ can promote a richer and more uniform distribution of TiC hard phases, and also optimize the precipitation and distribution of $M_{23}(C,B)_6$ eutectic carbides. The increase in hard phases is directly related to the enhancement of hardness and the improvement of wear resistance[18]. Due to its work hardening characteristics, the austenitic matrix can form a work hardening layer on the surface under abrasive wear conditions, effectively suppressing the propagation of microcracks and enhancing the wear resistance of the cladding metals. However, excessive addition of $Y_2O_3$ element can cause the microstructure of the cladding metals to become rough, which in turn weakens the wear resistance of the cladding metals.

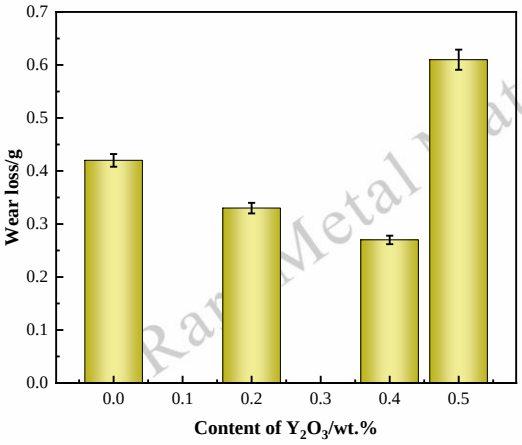


Fig. 9 Wear weight loss of cladding metals with different $Y_2O_3$ content

Fig. 10 shows the wear morphology of the cladding metals with different contents of $Y_2O_3$ added. When $Y_2O_3$ is not added, the plowing depth on the worn surface is relatively large, accompanied by obvious plowing wrinkles and peeling pits, and surface cracks are clearly visible. The addition of 0.2 wt.% nano-$Y_2O_3$ to the cladding metals resulted in a reduction in the number of surface wrinkles and peeling pits, as well as a reduction in the depth of plowing grooves. When the addition amount of $Y_2O_3$ increases to 0.4 wt.%, the depth of wear marks on the surface of the cladding metals is minimized and exhibits uniform distribution characteristics. At this point, there are no peeling pits, indicating that the wear resistance of the cladding metals reaches its optimal level. However, as the content of $Y_2O_3$ continues to increase, the depth of wear marks on the surface of the cladding metals deepens, and at the same time, debris and plowing wrinkles appear, indicating a decrease in wear resistance. There are two mechanisms for the formation of debris: micro cutting and local fracture peeling. A large number of plows indicate that the wear mechanism of the alloys is mainly abrasive wear. As shown in Tab. 4, region B is the $M_{23}(C, B)_6$ eutectic carbide embedded in the matrix $\gamma$ -Fe, and the high hardness $M_{23}(C, B)_6$ eutectic carbide plays a role similar to a wear-resistant skeleton. Region C is TiC, and the dispersed TiC hard phase particles hinder the movement of dislocations, contributing positively to the wear resistance. The appropriate addition of $Y_2O_3$ can promote the precipitation of TiC hard phase and adjust the distribution morphology of eutectic carbide $M_{23}(C,B)_6$. These changes have a significant positive impact on the wear resistance of the cladding metals, resulting in a significant improvement.

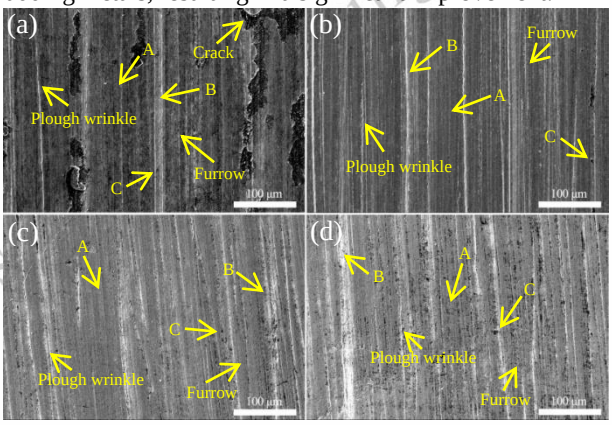


Fig.10 Wear morphology of cladding metals with different $Y_2O_3$ content: (a) 0 wt.% (b) 0.2 wt.%, (c) 0.4 wt.%, (d) 0.5 wt.%

Tab. 4 Energy spectrum analysis (wt.%)

| $Y_2O_3$ content | | B | C | Ti | Cr | Fe | Y |
|---|---|---|---|---|---|---|---|
| 0 wt.% | A | 3.99 | 5.81 | 0.63 | 15.21 | 74.36 | - |
| | B | 1.61 | 3.40 | 0.65 | 26.86 | 67.48 | - |
| | C | 2.65 | 11.84 | 42.63 | 12.87 | 30.01 | - |
| 0.2 wt.% | A | 5.55 | 4.48 | 0.85 | 13.86 | 75.12 | 0.14 |
| | B | 2.04 | 4.69 | 0.91 | 26.89 | 65.28 | 0.19 |
| | C | 2.41 | 14.55 | 47.20 | 10.11 | 25.73 | 0.20 |
| 0.4 wt.% | A | 5.51 | 4.52 | 0.96 | 11.53 | 77.17 | 0.31 |
| | B | 5.94 | 4.05 | 1.14 | 22.44 | 66.02 | 0.41 |
| | C | 3.94 | 9.83 | 46.02 | 11.57 | 28.27 | 0.37 |
| 0.5 wt.% | A | 5.50 | 5.79 | 1.38 | 11.68 | 75.27 | 0.38 |
| | B | 3.91 | 6.86 | 1.91 | 22.03 | 64.82 | 0.47 |
| | C | 3.38 | 9.48 | 48.51 | 10.65 | 27.49 | 0.49 |

Fig. 11 shows a schematic diagram of abrasive wear. The hard phase of cladding metals is mainly composed of TiC par-

ticles combined with $M_{23}(C,B)_6$ eutectic carbides. Among them, $M_{23}(C,B)_6$ eutectic carbides have high hardness and are uniformly embedded in the matrix in a regular grid shape, playing a role similar to a wear-resistant skeleton. In addition, a large amount of dispersed TiC hard phase particles also play a positive role in the overall wear resistance of the cladding metals. In the cladding metals without the addition of $Y_2O_3$, the precipitation amount of TiC hard phase is relatively limited, which limits the effective display of its wear resistance performance. On the contrary, when $Y_2O_3$ is appropriately introduced into the cladding metals, the precipitation amount of TiC hard phase significantly increases, and the distribution of hard phase is more uniform, and the spacing between particles decreases. The dispersed TiC hard phase particles hinder the movement of dislocations, contributing positively to the wear resistance. This structure prevents the abrasive from continuously cutting the substrate, effectively improving the wear resistance of the cladding metals.

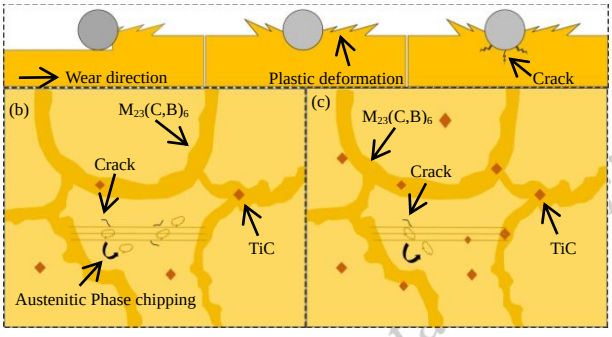


Fig. 11 The process of abrasive wear: (a) different processes, (b) low TiC precipitation, (c) high TiC precipitation

## 3 Conclusions

Fe-Cr-C-B-Ti-Y cladding metals was prepared using plasma cladding technology, and the microstructure and wear resistance of different $Y_2O_3$ content cladding metals were analyzed. Moreover, the mechanism of the wear process of cladding metals was analyzed. The following conclusion has been drawn:

1) In the formability analysis of cladding metals, the appropriate addition of $Y_2O_3$ can significantly improve the formability quality of the cladding metals. Especially when the $Y_2O_3$ content reaches 0.4wt.%, The cladding metal exhibits the best formability, with the wetting angle gradually decreases to 52.2 °.

2) There was no change in the phase composition for different $Y_2O_3$ content of the cladding metals. The microstructure in the cladding metals is still composed of austenite γ-Fe+$M_{23}(C,B)_6$ eutectic carbide+TiC hard phase. When the content of $Y_2O_3$ is 0.4 wt.%, the precipitation amount of TiC hard phase and $M_{23}(C,B)_6$ eutectic carbides is the highest, and the microstructure grains are the smallest.

3) Compared with not adding $Y_2O_3$, wear resistance and hardness of the cladding metals modified with $Y_2O_3$ are significantly improved. When the $Y_2O_3$ content reaches 0.4wt.%, The hardness of the cladding metals increased sharply to 89.7 HRC, with a hardness enhancement ratio of 47%. At the same time, the wear weight loss was reduced to the lowest, only 0.27 g, and the improvement in wear resistance was as high as 55.56%. The wear behavior of the cladding metals is mainly attributed to the abrasive wear mechanism, which involves micro cutting and plowing effects during the wear process.

4) The wear resistance of the deposited metal is closely related to the size, quantity, and distribution of the second phase. In the future, a comprehensive analysis can be conducted based on the research content. In addition, the wear resistance of the deposited metal with different welding passes can also be analyzed.

## References


1 Venkatesh B, Sriker K, Prabhakar V S V. Procedia Materials Science[J], 2015, 10: 527-532.
2 Li J., Kannan R., Shi M, et al. Metall Mater Trans B[J], 2020: 1291-1300.
3 E. Feldshtein, M. Kardapolava, O. Dyachenko. International Journal of Applied Mechanics and Engineering[J], 2018, 23(2): 851-862.
4 Debta M K, Masanta M .International Journal of Refractory Metals and Hard Materials[J], 2023: 106078.
5 Shi Z J, Liu S, Guo J, et al. Journal of Materials Science[J], 2019, 54: 10102-10118.
6 Zhang T G, Xiao H Q, Zhang Z Q, et al. Journal of Materials Engineering and Performance[J], 2020, 29(12): 8221–8235.
7 Zhang K M, Zou J X, Jun L I, et al. Transactions of Nonferrous Metals Society of China[J], 2012, 22(8):1817–1823.
8 Liu S, Shi Z J, Xing X L, et al. Materials Today Communications, 2020[J], 24: 101232.
9 Wang X H, Liu S S, Zhang M, et al. Tribology Transactions, 2020[J], 63(2): 345-355.
10 Liang X W, Su Y H, Yang T S, et al. JOM[J], 2023: 1-9.
11 X Y Ai, Z J Liu, Z X Zou. Crystals[J], 2023, 13: 1023.
12 Bramfit B L. Metallurgical Transactions[J], 1969, 1: 1978-1995.
13 Liu S, Zhang J, Wang Z J, et al. Materials Characterization[J], 2017, 132: 41-45.
14 Liu S, Zhou Y, Xing X, et al. Journal of Alloys and Compounds[J], 2017, 691(1): 239-249.
15 Debta M K, Masanta M. International Journal of Refractory Metals and Hard Materials[J], 2023.
16 Zhang T G, Xiao H Q, Zhang Z Q, et al. Journal of Materials Engineering and Performance[J], 2020, 29(12): 8221-8235.
17 Su Y H, Liang X W, Liu Y Q, et al. Acta Metallurgica Sinica (English Letters)[J], 2020, 33(07): 957-967.

18 Wang M L, Cui H Z, Wei N, et al. ACS Applied Materials & Interfaces[J], 2018, 10(4): 4250-4265.

# Y 含量对 Fe-Cr-C-B-Ti 熔覆金属成型性及摩擦磨损性能影响

郭建波[1]，刘政军[1]，苏允海[1*]

(1. 沈阳工业大学材料科学与工程学院，辽宁 沈阳 110870)

**摘　要**：磨损、腐蚀、疲劳构成了机械零件失效的三种形式，其中机械零件的磨损造成的能源消耗和经济损失尤为严重。通过等离子堆焊的方法制备 Fe-Cr-C-B-Ti-Y 系耐磨熔覆金属。采用 MLS-23 型橡胶轮式湿砂磨损试验机分析了熔覆金属的磨损性能。采用 XRD、SEM、EBSD 和 TEM 分析了熔覆金属的物相组成和显微组织，并对合金的强化机理和磨损机理进行了探讨。结果表明：Fe-Cr-C-B-Ti-Y 熔覆金属中显微组织由奥氏体 γ-Fe+$M_{23}(C,B)_6$ 共晶碳化物+TiC 硬质相组成。随着 $Y_2O_3$ 添加量的增多，熔覆金属的硬度与磨损量呈现先增加后减小的变化趋势。当 $Y_2O_3$ 含量为 0.4 %时，TiC 硬质相与 $M_{23}(C,B)_6$ 共晶碳化物析出量最多，组织晶粒最为细小。熔覆金属成型性最好，润湿角最小，为 52.2°。此时，熔覆金属的洛氏硬度值为 89.7 HRC，磨损失重为 0.27g。熔覆金属的磨损机制主要为磨粒磨损，材料的去除过程为显微切削与犁沟。

**关键词**：Fe-Cr-C-B；熔覆金属；纳米Y2O3；陶瓷相；耐磨性

作者简介：郭建波，男，1980 年生，博士研究生，沈阳工业大学材料科学与工程学院，辽宁 沈阳 110870，电话：18109859601，E-mail: GUOJIANBO@126.COM